JACS
JOURNAL OF THE AMERICAN CHEMICAL SOCIETY
Article
pubs.acs.org/JACS

Structural Modulation in the High Capacity Battery Cathode Material $LiFeBO_3$

Yuri Janssen,[†] Derek S. Middlemiss,[‡] Shou-Hang Bo,[†] Clare P. Grey,*[,†,‡] and Peter G. Khalifah*[,†,§]

[†]Department of Chemistry, SUNY Stony Brook, Stony Brook, New York 11794, United States
[‡]Department of Chemistry, University of Cambridge, Lensfield Road, Cambridge, CB2 1EW, United Kingdom
[§]Chemistry Department, Brookhaven National Laboratory, Upton, New York 11973, United States

Supporting Information

ABSTRACT: The crystal structure of the promising Li-ion battery cathode material $LiFeBO_3$ has been redetermined based on the results of single crystal X-ray diffraction data. A commensurate modulation that doubles the periodicity of the lattice in the *a*-axis direction is observed. When the structure of $LiFeBO_3$ is refined in the 4-dimensional superspace group $C2/c(\alpha 0\gamma)00$, with $\alpha = 1/2$ and $\gamma = 0$ and with lattice parameters of $a = 5.1681$ Å, $b = 8.8687$ Å, $c = 10.1656$ Å, and $\beta = 91.514°$, all of the disorder present in the prior $C2/c$ structural model is eliminated and a long-range ordering of 1D chains of corner-shared LiO_4 is revealed to occur as a result of cooperative displacements of Li and O atoms in the *c*-axis direction. Solid-state hybrid density functional theory calculations find that the modulation stabilizes the $LiFeBO_3$ structure by 1.2 kJ/mol (12 meV/f.u.), and that the modulation disappears after delithiation to form a structurally related $FeBO_3$ phase. The band gaps of $LiFeBO_3$ and $FeBO_3$ are calculated to be 3.5 and 3.3 eV, respectively. Bond valence sum maps have been used to identify and characterize the important Li conduction pathways, and suggest that the activation energies for Li diffusion will be higher in the modulated structure of $LiFeBO_3$ than in its unmodulated analogue.

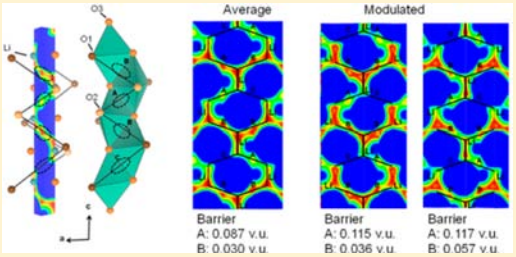

1. INTRODUCTION

Rechargeable Li-ion batteries are a key component in mobile electronics, and are expected to play a central role in the commercialization of hybrid electric vehicles and plug-in hybrid vehicles. Battery performance is the major factor limiting the utilization of electric vehicle technologies.[1] The development of new Li-ion battery systems will potentially provide the necessary breakthrough improvements in battery energy density, power density, lifetime, and cost that will allow for widespread adoption of electric vehicle technology. There is a pressing need to understand and overcome the limitations of current Li-ion battery systems with regard to these criteria.

An important new generation of low-cost cathode materials for Li-ion batteries have recently been produced by combining phosphate oxoanion groups with the abundant and inexpensive transition metal iron.[2−4] While Fe^{2+} does not typically cycle at a sufficiently high potential to enable the high energy density required for many commercial applications, the inductive (electron-withdrawing) effect of the oxoanion phosphate group substantially raises the redox potential of $LiFePO_4$ relative to oxide analogues.[2,5,6] As a result, $LiFePO_4$ cathodes can have a relatively large specific capacity (170 mAh/g) and operate at a relatively high potential of 3.4 V, resulting in a specific energy density that approaches that of oxide cathode materials such as $Li(Ni_{1/3}Mn_{1/3}Co_{1/3})O_2$.[7] Inspired by the successful development of $LiFePO_4$, the search for improved cathode materials has turned to other oxoanion systems with potentially larger energy densities. One such system is $LiFeBO_3$, where the higher charge/mass ratio of the BO_3^{3-} groups leads to a theoretical charge capacity of 220 mAh/g, about 30% larger than that of PO_4^{3-}-based $LiFePO_4$.

Although early attempts to access the full capacity of $LiFeBO_3$ at room temperature were unsuccessful,[8−10] significant performance improvements have recently been achieved.[11,12] In 2010, Yamada et al.[11] showed that the exclusion of air and moisture from all processing steps can lead to a reversible capacity of 190 mAh/g at potentials of 2.8−3.2 V (vs Li^+/Li), and suggested that the volume changes on cycling are very small (only 2−3%). A similar performance was achieved within our group[13] in the course of a more thorough investigation of the degradation mechanism of $LiFeBO_3$. It has been demonstrated by others that the isostructural (monoclinic) form of $LiMnBO_3$ can also be reversibly cycled at a potential of about 3.7 V, although a smaller fraction of the theoretical capacity could be accessed.[14] Furthermore, Yamada et al.[15] have studied the solid solution $LiFe_{1-x}Mn_xBO_3$ cathode, finding that the addition of Mn produces a second voltage plateau at the expected 3.7 V. The electronic and ionic conductivity of $LiFeBO_3$ are not well established although the electrical conductivity has been reported as 1.5×10^{-4} S/cm (ref 9). Theoretical calculations on $LiMBO_3$ (M = Fe, Mn, Co) compounds have been carried out,[14−16] and suggested strongly one-dimensional Li-diffusion pathways with an activation

Received: February 25, 2012
Published: June 18, 2012

energy of 440 meV for $LiFeBO_3$.[16] However, these calculations were performed without knowledge of the full four-dimensional crystal structure of $LiFeBO_3$, and instead used a model based on the disordered $LiZnBO_3$ structure type as a starting point.

The published crystal structure of $LiFeBO_3$[8] that is commonly cited in the literature was determined from a single crystal X-ray diffraction study, and was effective in fitting the intensities of the observed reflections (R_1 = 0.050). On the basis of this refinement, it was concluded that $LiFeBO_3$ crystallizes in the $LiZnBO_3$-type structure,[17] with the monoclinic space group $C2/c$ (#15) and lattice parameters a = 5.169 Å, b = 8.924 Å, c = 10.138 Å, and β = 91.39°. In this structure, both Li and Fe sit in apparent trigonal bipyramidal coordination, with both Li (52%/48%) and Fe (72%/28%) refined as partially occupying a position above or below the equatorial plane of their respective bipyramids. For prior ab initio calculations, which cannot simply incorporate disorder, an ordered structural model was generated to investigate the isostructural compound $LiMnBO_3$,[14] in which both Li and Mn cations were situated in a tetrahedral-like coordination environment.

On the basis of our single-crystal X-ray diffraction experiments, it is shown that the actual structure of $LiFeBO_3$ can be best described in the 4-dimensional commensurately modulated superspace group $C2/c(\alpha 0\gamma)00$, with α = 1/2 and γ = 0. This new description eliminates both the disorder and the large atomic displacement parameters that were found in the prior $C2/c$ model, and results in a substantially different Li coordination environment whose impact on Li diffusion processes can be explored. On the basis of this new structure, bond-valence calculations were used to assess Li-diffusion pathways and first-principles density functional theory (DFT) calculations were carried out. These calculations apply hybrid density functionals for the first time that include a finite admixture of Fock exchange to this promising cathode material, building upon the demonstrable accuracy of such functionals in application to other transition metal compounds.[18] They provide detailed insights into the variations in electronic structure that occur on delithiation. The optimized structural parameters and energetics of the new and previously suggested structures for $LiFeBO_3$ are compared.

2. EXPERIMENTAL METHODS

2.1. Crystal Growth. A procedure similar to that described by Legagneur et al.[8] was used to prepare $LiFeBO_3$ single crystals. $LiBO_2$ and $FeC_2O_4{\cdot}2H_2O$ powders were mixed in a molar ratio of 10:1 and ground using an agate mortar and pestle. This precursor sample was loaded into a steel crucible, and heated to 1100 °C for 10 h in a 3.125 in. inner diameter mullite tube furnace under a continuous flow of N_2 gas. The furnace was subsequently cooled over 30 h to 800 °C, after which the furnace was turned off and allowed to cool naturally to room temperature. The crucible contained a mixture of rod-like light-gray transparent $LiFeBO_3$ and white $LiBO_2$ crystals, as confirmed by powder diffraction studies on ground crystals.

2.2. Single-Crystal X-ray Diffraction. The crystal structure of $LiFeBO_3$ was determined from single-crystal X-ray diffraction data collected at room-temperature with an Oxford Diffraction Gemini diffractometer using Mo K_α radiation. Data reduction and empirical absorption corrections were performed using the computer-program package CrysAlisPro v171.33.55. The crystal structure was solved using the charge-flipping method as implemented in the computer program Superflip,[19] and then refined using the computer program Jana2006.[20]

2.3. Bond-Valence Model Calculations. Bond-valence sum (BVS) calculations[21] were used to analyze bonding within the crystal structure of $LiFeBO_3$. To evaluate possible Li-ion diffusion paths, three-dimensional bond-valence sum maps for Li in $LiFeBO_3$ were calculated using a local computer program based on the Crystallographic Fortran Modules Library,[22] using its structural calculations and file-handling capabilities. In these calculations, the positions of O atoms were used to calculate the valence of Li atoms positioned at each point on a 3D grid inside the unit cell using the BVS parametrization recommended by Adams.[23] The energy of Li at each grid point is expected to increase monotonically as the valence deviates from the ideal lithium value of +1, albeit in a nontrivial manner. The absolute difference (ΔV_{xyz}) between the ideal Li valence and the bond-valence sum calculated at each point (V_{xyz}) was represented in a 3D plot, providing phenomenological insights into likely diffusion pathways via an examination of isosurfaces of ΔV_{xyz} set at the minimal values necessary to connect Li sites into a continuous network. Such isosurfaces should, in effect, highlight the lowest energy positions of Li within the anion framework. This method has previously been applied to successfully predict Li-diffusion pathways in $LiFePO_4$ and other battery materials.[24]

2.4. Computational Methods. First-principles DFT calculations were performed within the CRYSTAL06 code utilizing a linear combinations of atomic orbitals approach.[25] The B3LYP hybrid functional[26] was used throughout, given its previous satisfactory performance for the electronic structure and band gaps of a broad range of materials[27] and for the properties of transition metal compounds in particular.[18] The atom-centered basis sets used here comprise a series of shells each composed of a fixed contraction of Gaussian primitive functions, of the overall form 1s(5) 2sp(1) 3sp(1) 3d(1) for Li, 1s(6) 2sp(2) 3sp(1) 3d(1) for B, 1s(8) 2sp(4) 3sp(1) 4sp(1) 3d(1) for O, and 1s(8) 2sp(6) 3sp(4) 4sp(1) 5sp(1) 3d(4) 4d(1) for Fe; the value in parentheses indicates the number of primitives within each shell. The Li, Fe, and O sets were unmodified from their previous use in a broad range of compounds, while an increase in the B 3sp shell exponent to 0.1643 atomic units (au) was found to be necessary to avoid convergence difficulties in the self-consistent field.[28] Reciprocal space was sampled upon Monkhorst-Pack meshes of dimensions 8 × 8 × 4 for the smaller published $C2/c$ cell, and 4 × 4 × 4 for the larger cell proposed here, providing adequate convergence in total energies for the present purposes. Coulomb and exchange integral series tolerances of 10^{-7}, 10^{-7}, 10^{-7}, 10^{-7}, and 10^{-14} were used, as defined in the CRYSTAL06 documentation,[25] again providing adequate convergence. Full geometry optimizations (atomic positions and cells) were undertaken for all structures, strictly preserving the initial space group symmetries. A quasi-Newton algorithm was applied, with root-mean-squared (rms) convergence tolerances of 0.0003 and 0.0012 au for forces and displacements, respectively (the tolerances for maximum components set at 1.5 times the respective rms values), and a total energy tolerance of 10^{-7} au. All optimizations were restarted at least once to avoid problems due to fixed integral series lengths. Distributions of charge and spin densities were analyzed, and atomic projections for densities-of-states plots defined via Mulliken population analyses of the converged wave functions. A ferromagnetic high-spin alignment consistent with four and five unpaired electrons per notional Fe^{2+} and Fe^{3+} site, respectively, was used throughout. Tests applying a range of states of spin order confirm the stability of the ferromagnetic state in $LiFeBO_3$, while $FeBO_3$ is predicted to be an antiferromagnet. However, the magnetic energy differences in the latter phase amount to less than 1.5 kJ/mol in all cases.

3. RESULTS AND DISCUSSION

3.1. Idealized Structure. As a first step toward understanding the atomic arrangements in $LiFeBO_3$, it is instructive to consider the symmetry of a geometrically ideal arrangement with the same connectivity of atoms but with ideal coordination polyhedra about each cation and with optimal metal−oxygen (M−O) bond lengths (derivation in Supporting Information). The $LiFeBO_3$ structure can be deconstructed into four symmetrically equivalent layers of cations that stack in the c-

dx.doi.org/10.1021/ja301881c | J. Am. Chem. Soc. 2012, 134, 12516−12527

axis direction at heights of z = 1/8, 3/8, 5/8, and 7/8, as shown in Figure 1. The stacking itself is shown in Supporting Information Figure S1. When all atoms are placed at ideal positions within this plane, each O atom has six nearest-neighbor O atoms within the plane in a distorted hexagonal arrangement characteristic of close-packing. Within every idealized layer, there is a three-fold symmetry axis that passes through each of the three cation sites. Although each individual layer is compatible with the symmetry of a trigonal lattice, the three-fold axes in subsequent planes do not coincide when the layers are stacked in the manner observed for $LiFeBO_3$ and the lattice symmetry must instead be described using a lower symmetry orthorhombic cell, whose relationship to the trigonal planar lattice is marked in Figure 1. Although the unit-cell dimensions are compatible with a C-centered orthorhombic lattice, the actual stacking between layers is not and the true space group symmetry of the idealized $LiFeBO_3$ structure is monoclinic ($C2/c$, #15) where the β angle is exactly 90°. The previously reported space group symmetry[8] of $LiFeBO_3$ is essentially identical to that just discussed, but with a β angle of 91.4° differing only slightly from the ideal value.

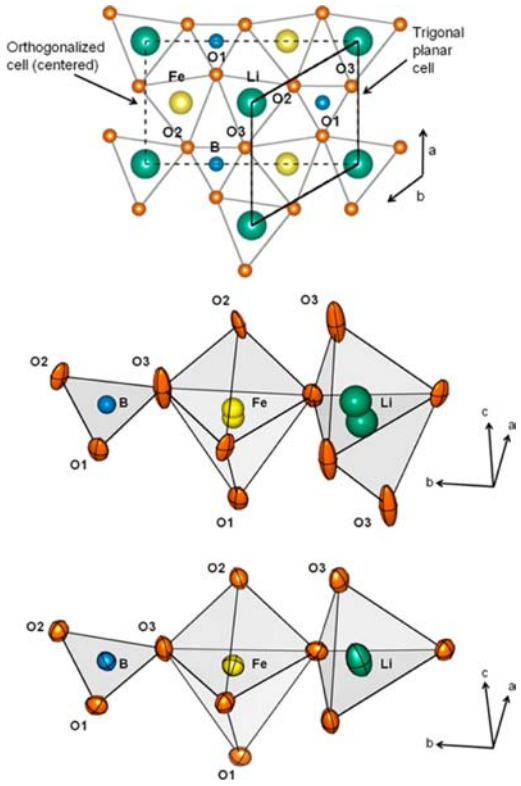

Figure 1. Top: Idealized 2D layer of $LiFeBO_3$. Its structure is described by the trigonal plane group $P3$ with a lattice parameter of a = 5.066 Å. Also displayed is the orthogonalized centered unit cell with a = 5.066 Å, b = 8.774 Å. Center: Literature $LiFeBO_3$ structure including anisotropic displacement for O atoms. The Li and Fe sites are split, and the O3 ellipsoid is anomalously elongated. Bottom: $LiFeBO_3$ fragment from present modulated superstructure. The Fe and Li sites are no longer split, all O atoms have similar displacement ellipsoids, and Li sits within a long-range ordered tetrahedral coordination environment.

3.2. Reported Structure. The crystal structure of $LiFeBO_3$ determined from an earlier single crystal diffraction experiment[8] is shown in Figure 1, and reveals that this compound has a framework which is potentially suitable for battery applications. Li cations are found within a trigonal bipyramidal arrangement of O anions, although the Li ions were reported to be displaced away from the center and disordered in an approximately 50/50 manner over two split sites in a manner that suggests the Li are actually in tetrahedral coordination. The Fe cations are similarly located within a trigonal bipyramidal site, and their position was also reported to be split, though in an approximately 70/30 manner with a much smaller displacement from the center of the bipyramid that suggests a higher coordination number of 5. The Fe and Li coordination polyhedra are connected into one-dimensional chains, allowing a potential low-resistance pathway for both electronic ([110] direction) and ionic conductivity ([001] direction). The B cations are found in BO_3^{3-} oxoanion groups, with the trigonal planar coordination expected for such groups. Oxygen atoms are arranged in what are essentially close-packed layers, although substantial distortions are present due to the differently sized cations found in each layer. There are three distinct O atomic positions, O1, O2, and O3, where the last was reported to have a strongly elongated displacement ellipsoid. Although the original structural refinement had a very low R-value (a result that could be reproduced by using crystals grown in this study), the fact that three of the six atomic positions exhibit anomalous displacements or splitting in the c-axis direction suggests that this crystallographic description of the $LiFeBO_3$ structure is incomplete.

3.3. Single-Crystal X-ray Diffraction. Single-crystal X-ray diffraction experiments on multiple crystals obtained from different growth batches indicate that the published structure of $LiFeBO_3$ requires amendment. Crystals typically lacked well-defined facets but still generated high quality diffraction data. While automatic indexing and space-group determination routines supplied the literature unit cell with $C2/c$ space group symmetry, visual inspection of reciprocal lattice planes reconstructed from the diffraction data showed additional, weaker, satellite reflections at half-integer h-values that are indicative of a unit cell with a doubled a-axis period (Figure 2). Together with the stronger reflections, the satellite reflections could be used to define a doubled a-axis unit cell that uniquely obeyed the reflection conditions for the conventional space group $P2_1/c$ (#14). In this definition, however, there are systematic absences occurring at locations not predicted by any of the 230 three-dimensional (3D) space groups, indicating that $P2_1/c$ is an inadequate description of the symmetry of this phase. Higher dimensional space groups were tested using the Jana2006 software, and it was determined that all observed reflections fulfill the reflection conditions for the 4D superspace group $C2/c(\alpha 0\gamma)00$ (which can equivalently be represented in a $C2/c(\alpha 0\gamma)0s$ setting), a space group that belongs to the (3 + 1)D subset of 4D space groups.[29] This is a commensurately modulated space group with the $^1/_2 00$ modulation vector generating the diffraction peaks occurring at half-integer h indices that effectively double the period of the a-axis translational symmetry. The superspace group $C2/c(\alpha 0\gamma)00$, which will herein be abbreviated as $C2/c(^1/_2 00)00$, was used subsequently for structure solution and refinement. Table 1 summarizes the results of the diffraction experiment, and Figure 2 shows the reciprocal space relationships linking the $C2/c$ subcell, the $P2_1/c$ supercell, and the $C2/c(^1/_2 00)00$ superspace group unit cell, all relative to the $h0l$ reciprocal lattice plane of $LiFeBO_3$ reconstructed from the experimental single crystal diffraction data.

dx.doi.org/10.1021/ja301881c | J. Am. Chem. Soc. 2012, 134, 12516–12527

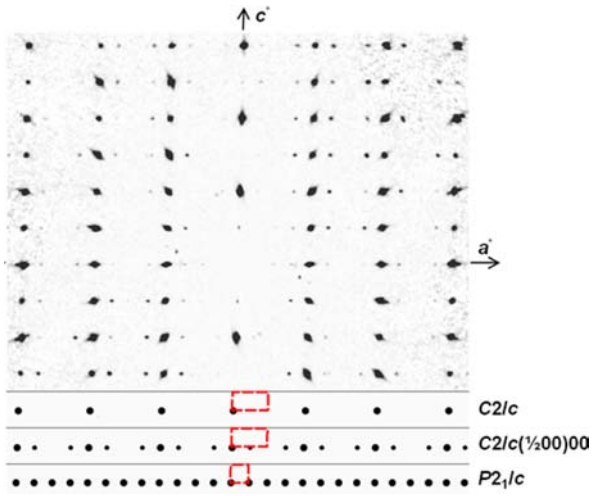

Figure 2. The (*h*0*l*) reciprocal lattice plane for $LiFeBO_3$, and spot patterns that result from three putative space groups. The originally proposed $C2/c$ cell cannot index the weak spots resulting from the modulation, while the alternative $P2_1/c$ cell indexes all observed spots but predicts many more spots than are observed. The superspace group $C2/c(^1/_2 00)00$ describes a commensurately modulated $C2/c$ lattice with a propagation vector that doubles the cell in the *a*-direction and a symmetry which predicts both the extra reflections (with *m* indices of ±1) and the systematic absence of every fourth column of reflections in this *h*0*l* plane.

The structure of $LiFeBO_3$ was readily solved and refined in superspace group $C2/c(^1/_2 00)00$. This modulated structure was first refined with all positions fully occupied, allowing for modulation only on the positional parameters. No significant improvement in the refinement was found by allowing for partial occupation of any of the atom sites, nor by permitting modulations of the anisotropic displacement parameters. The refined average atomic positions, the Fourier coefficients for the modulation of the atomic positions, and the respective atomic displacement parameters are given separately in Tables 2 and 3 and Supporting Information Table S2. Although the conventional 3D space group $P2_1/c$ is not suitable for refining the structure of $LiFeBO_3$ due to missing symmetry constraints, it does suffice to completely describe the atomic positions resulting from the commensurate modulation. The $P2_1/c$ description of the $LiFeBO_3$ structure requires one-third more parameters to completely specify atomic positions than the modulated description [72 variables in $P2_1/c$ versus 54 in $C2/c(^1/_2 00)00$]. As a result, structural refinements carried out in $P2_1/c$ symmetry will suffer from correlations that occur when the *x*, *y*, and *z* positional parameters are not all independent. Nevertheless, the $P2_1/c$ description of the modulated structure provides a useful and complete description of the atomic positions in $LiFeBO_3$, with particular relevance to software that cannot readily represent modulated structures (i.e., standard structural visualization and density functional theory simulation packages), and is given in Supporting Information Table S3.

Despite the complex crystallography required for the solution and refinement of the modulated structure, the physical effects of the $LiFeBO_3$ modulation are simple to describe. As compared with the average structure, only the Li and O3 atoms are strongly influenced by the modulation, and their displacements are largely confined to the *c*-axis direction. The positions of the remaining atoms are essentially unmodulated. The relative amplitudes of the sinusoidal displacements

Table 1. Crystal Data and Structure Refinement for $LiFeBO_3$ at Room Temperature

Temperature (K)	293
Crystal volume (mm^3)	2.2×10^{-3}
Wavelength (Å)	0.71073
Crystal system	monoclinic
Superspace group	$C2/c(\alpha 0 \gamma)00$
Modulation dimension, vector	1, $(^1/_2 00)$
a (Å)	5.1681(6)
b (Å)	8.8687(8)
c (Å)	10.1656(9)
β (°)	91.514(8)
$V(Å^3)$, *Z*	465.77(8), 8
Experimental density (g/cm^3)	3.47
Absorption coefficient (mm^{-1})	6.177
F(000)	232
θ range for data collection (°)	3.66 to 45.83
Index ranges	$-10 \le h \le 10$
	$-17 \le k \le 17$
	$-14 \le l \le 20$
	$-1 \le m \le 1$
Reflections collected	48940
Unique data	7960
Parameters	92
Completeness to 0.5 Å	99.92%
R_{int}	0.052
Refinement method	F^2
$R(F)$ ($I > 3\sigma$) total reflections	0.0293
$wR(F^2)$ total reflections	0.0732
$R(F)$ ($I > 3\sigma$) main reflections	0.0230
$wR(F^2)$ main reflections	0.0578
$R(F)$ ($I > 3\sigma$) satellites	0.0647
$wR(F^2)$ satellites	0.1357
Extinction coefficient	0.0380(30)
Largest diff. peak and hole ($e/Å^3$)	0.64 and −0.80

Table 2. Average Atomic Sites for $LiFeBO_3$ about Which the Modulation Occurs

atom[a]	*x*	*y*	*z*	U_{eq} ($Å^2$)
Li	0.1625(3)	0.00227(17)	0.12634(12)	0.0181(4)
Fe	0.161281(18)	0.336043(11)	0.124577(9)	0.01014(2)
B	0.66570(13)	0.16785(7)	0.12523(6)	0.00745(12)
O1	0.40492(9)	0.16133(5)	0.09233(4)	0.00926(9)
O2	0.78031(9)	0.30415(5)	0.15750(4)	0.00905(9)
O3	0.81256(10)	0.04041(6)	0.12547(5)	0.01168(11)

[a]All atoms are found at the 8*f* Wykoff position.

resulting from the modulation are shown in Figure 3 and are specified by the Fourier coefficients given in Table 3. The net effect of the commensurate modulation is to specify four distinct locations (labeled *a*–*d*) for each of the six atoms (Li, Fe, B, O1, O2, O3) originally occurring in the average $C2/c$ structure of Legagneur. The commensurately modulated structure, therefore, describes a structure of $LiFeBO_3$ which is completely ordered (Figure 4), suggesting that the disorder in the earlier description is an artifact of the crystallographic symmetry used to describe the diffraction data.

A comparison between the present modulated and previously described average structure finds that the changes are generally small. Lists of relevant bond distances (Supporting Information Table S4) and angles (Supporting Information Table S5) are reported. The bond distances among the four variants of the

dx.doi.org/10.1021/ja301881c | J. Am. Chem. Soc. 2012, 134, 12516–12527

Table 3. Fourier Coefficients of Displacement Generated by the Modulations in $LiFeBO_3$[a]

atom		x	y	z
Li	sin	−0.0031(4)	−0.0089(2)	**−0.0386(3)**
	cos	0.0018(4)	0.0058(3)	**0.0217(3)**
Fe	sin	−0.00186(3)	−0.003274(15)	−0.000451(12)
	cos	−0.00556(2)	0.000962(18)	−0.004399(11)
B	sin	−0.0002(2)	−0.00024(11)	0.00347(9)
	cos	−0.00090(18)	0.00131(13)	0.00378(7)
O1	sin	0.00064(12)	0.00128(7)	−0.00040(5)
	cos	0.00133(12)	0.00093(7)	0.00008(5)
O2	sin	0.00114(12)	0.00123(8)	0.00091(5)
	cos	−0.00243(12)	0.00183(8)	−0.00062(5)
O3	sin	−0.00419(13)	−0.00113(8)	**0.01773(6)**
	cos	−0.00088(13)	0.00065(8)	**0.01023(7)**

[a]The only atoms that are substantially modulated are Li and O3, with their only significant modulation amplitudes (emphasized in bold) occurring in the *c*-axis direction.

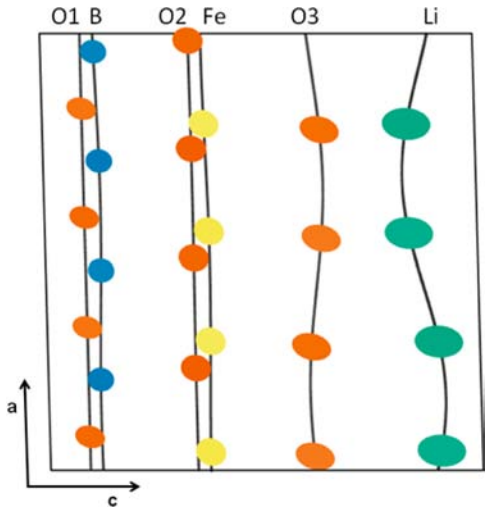

Figure 3. Schematic projection of atomic displacement ellipsoids onto the *ac* plane of $LiFeBO_3$ for a unit cell doubled in the *a*-direction. Note that the only two atoms which exhibit large displacements (Li and O3) do so in a cooperative manner which magnifies changes in the Li−O3 bond lengths and generates nearly regular tetrahedral coordination for Li.

original sites are quite similar, with a spread that is at most 0.08 Å, but which is typically much smaller, at approximately 0.02 Å.

The major effect of the modulation is to modify the coordination environment of Li, changes in which are of critical importance in understanding the electrochemical performance of $LiFeBO_3$ as a cathode. The modulations move the Li atoms out of the equatorial planes of their trigonal bipyramids, leading ultimately to tetrahedral coordination. At the same time, the O3 atom displacement shortens the apical axis of the Li tetrahedra relative to that occurring in the original bipyramid. Both changes serve to enhance Li−O bonding relative to that anticipated in trigonal bipyramidal coordination, a conclusion supported by the bond valence sum calculations discussed below. The LiO_4 tetrahedra have a consistent asymmetry, with the apical Li−O bond (parallel to the *c*-axis) being approximately 0.1 Å longer than the other three bonds. The refined Li−O bond distances and angles are in good agreement with those occurring in numerous other Li-containing oxides described in Pearson's Crystal Database.[30]

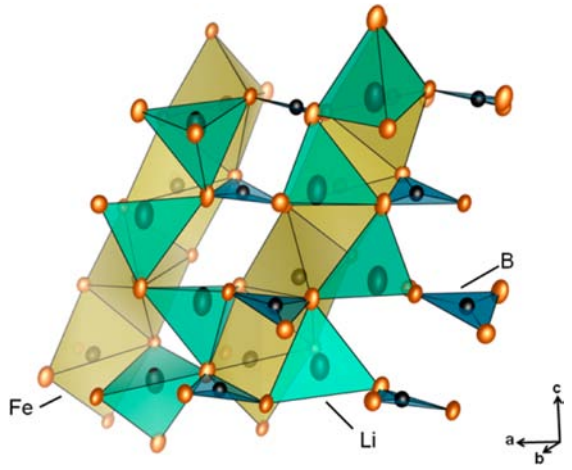

Figure 4. The commensurately modulated structure of $LiFeBO_3$. Note the corner-sharing chains of LiO_4 tetrahedra running parallel to the *c*-axis [001], with their apexes all pointing in the same direction within each chain but flipping between consecutive chains when moving in the *a*-axis direction. FeO_5 bipyramids are arranged in edge-sharing chains which run in the $[10\bar{1}]$ direction.

As seen in Figure 4, the modulation has a smaller effect on the geometry of the Fe trigonal bipyramids, manifesting itself mainly in a slight tilting of the equatorial planes of the bipyramids due to displacement of the O3 atoms in their respective normal directions. Fe atoms are found to be contained within the equatorial planes of the trigonal bipyramids. The equatorial Fe−O bond lengths of ∼2.00 Å are quite homogeneous and are substantially shorter than the apical Fe−O bonds. An asymmetry between the shorter (∼2.20 Å) and longer (∼2.30) apical Fe−O bonds arises in three of the four types of FeO_5 bipyramids present in the modulated structure, while, in the fourth FeO_5 bipyramid, the asymmetry is not present and both bonds are approximately 2.25 Å in length. The modulation also tilts the BO_3 triangles via the displacement of O3 atoms, but the B−O bonding remains regular and is very consistent with database structures.[30]

Although the tetrahedral coordination of Li could potentially be inferred from prior structural and theoretical work, the present modulated structure solution and refinement in superspace group $C2/c(^1/_2 00)00$ allows the coordinated displacements of the Li and O3 atoms to be resolved. This coherent displacement results in the formation of corner-sharing chains of LiO_4 tetrahedra that run parallel to the *c*-axis. The tetrahedra comprising each [001] chain all have their apical O3 oxygens pointing in the same direction, denoted up or down, and correspond to Li occupying the tetrahedron formed by the oxygens at either the top or bottom of a trigonal bipyramid. A long-range ordering of tetrahedral chains occurs within the *ab*-plane (orthogonal to the chains) in which the orientation of tetrahedra is maintained along the *b*-axis but flips between successive chains in the *a*-axis direction. This is exactly the direction of the modulation propagation vector of $^1/_2 00$, and the chain ordering is apparent in Figure 4, and is further emphasized in Supporting Information Figure S2.

3.4. BVS Analysis of Coordination and Bonding. The structural modulation revealed in $LiFeBO_3$ clearly modifies the cation coordination environments, and it is therefore important to understand the effect these changes may have on the binding of Li within this material. Changes in the strength and geometry of Li−O bonding have the potential to strongly

dx.doi.org/10.1021/ja301881c | J. Am. Chem. Soc. 2012, 134, 12516−12527

Table 4. Bond Valence Sums for Average Structure and Modulated Structure $LiFeBO_3$[a]

average structure		modulated structure							
cation	BVS (v.u.)	cation	BVS (v.u.)	cation	BVS (v.u.)	cation	BVS (v.u.)	cation	BVS (v.u.)
Li	1.079	Li1a	1.085	Li1b	1.049	Li1c	1.084	Li1d	1.025
Fe	1.946	Fe1a	1.929	Fe1b	1.944	Fe1c	1.936	Fe1d	1.941
B	2.970	B1a	2.960	B1b	2.952	B1c	2.949	B1d	2.958

[a]The bond-valence sums $V = \sum_n S$ were obtained by summing bond-valences $S = \exp((R_0 - R)/b)$, over the cation coordination with parameters R_0 and b from Brese and O'Keeffe,[31] and with experimental bond lengths.

influence Li diffusion, a topic that will be discussed more later. Insight into the factors underlying the presence of the structural modulation can be obtained via BVS analysis of the chemical bonds within the structure. The BVS method works by estimating the contribution of each coordinated anion to the valence of the central cation assuming a valence contribution that decreases exponentially with increasing bond length. Thus, the relative importance of different M−O bonds to overall phase stability may be assessed (M = Li, Fe, B for $LiFeBO_3$). Furthermore, the valences of the central Li and Fe cations of the framework groups can be estimated using empirical parameters derived from an analysis of a database of accurately determined crystal structures. If the valence calculated using the BVS method deviates substantially from that expected on the basis of charge balance, it is likely that the cation is overbonded or underbonded, situations which both indicate an nonideal (higher energy) coordination environment.

The $LiFeBO_3$ modulation predominantly affects the Li and O3 atoms, and their atomic sites are therefore a good starting point for comparing the unmodulated (average) and modulated structures. The results of BVS calculations using the empirical parameters of Brese and O'Keefe[31] are given in Table 4. For Li, the calculations were performed with trigonal bipyramidal coordination for the average structure and with tetrahedral coordination for the modulated structure. All valences in both structural models fall within 0.1 v.u. of the ideal values of 1+, 2+, and 3+ for Li, Fe, and B, respectively, indicating that both structures are viable to within the precision of the method. A further test of stability is provided by the global instability index (GII)[21] with values $GII = 0.044$ and 0.047, for the averaged and modulated structure, respectively. Both of these values are smaller than those often calculated for incorrect ($GII > 0.2$) or strained ($GII > 0.1$) structures, indicating that both structural models may be considered reasonable. The difference in GII values for the average and modulated structures is small, which anticipates that the energy difference between the two structures will also be small, a qualitative finding in agreement with the direct first principles calculations presented below.

A closer look at the individual bond valences given in Supporting Information Table S6 provides further insights. The differences for B and Fe atoms between the average and modulated structures are small. For B atoms in trigonal coordination, the individual bond-valences are similar to within a few percent and thus obey both the equal valence and the maximum symmetry principles proposed by Brown.[21] Meanwhile, for the trigonal-bipyramidally coordinated Fe atoms, the planar bond valences are all close to 0.47 v.u., whereas the axial bond valences are close to 0.26 v.u., consistent with stronger bonding within, rather than between the planes. The individual bond valences for Li in the trigonal bipyramidal coordination of the average structure are approximately 0.32 v.u. for the strong planar bonds, but fall to only approximately 0.05 v.u. for the axial bonds, suggesting that the Li coordination at this position might be more accurately regarded as trigonal rather than trigonal bipyramidal. The modulation in the present structure, meanwhile, decreases the separation between Li and O3 sites and results in tetrahedral Li coordination, as discussed above. The new bond valences for the shorter 'planar' bonds are about 0.29 v.u. while the valence of the single longer axial bond is about 0.18 v.u., so that the valences are more equal. The principle of maximum symmetry is maintained, since, first, substantial displacements occur only for those atoms necessary to yield ordered Li tetrahedra, namely, Li and O3, and second, the symmetry of the superspace group $C2/c(^1/_2 00)00$ is only one step lower than that of space group $C2/c$ experimentally observed earlier[8] and derived above for an idealized structure. These observations about the stability of $LiFeBO_3$, obtained through empirical BVS analysis, are also supported by the results of more quantitative DFT calculations, discussed below.

3.5. Optimized Structures and Relative Energetics. DFT calculations provide an opportunity to investigate the relative energies of $LiFeBO_3$ both in the presence of and lacking the structural modulation, providing insight into the forces driving the structural distortion. For the calculations, first the modulated $C2/c(^1/_2 00)00$ structure was transformed into the equivalent doubled a-axis $P2_1/c$ unit cell discussed above. The use of space group $P2_1/c$ circumvented the strict enforcement of the $C2/c(^1/_2 00)00$ symmetry restrictions, although a check of the diffraction pattern simulated on the basis of the final DFT optimized structure showed that there was not a large deviation from this symmetry after optimization. Next, total energies and structures were compared to an optimized unmodulated model (Figure 5, left) based on that of Legagneur et al.[8] as reported by Yamada et al.,[11] in which Li and Fe ions were each placed initially at the center of the trigonal bipyramids formed by the adjacent O anions. Finally, the most likely $FeBO_3$ structure resulting from the delithiation of modulated and unmodulated $LiFeBO_3$ was determined by removing Li from these structures and reoptimizing their

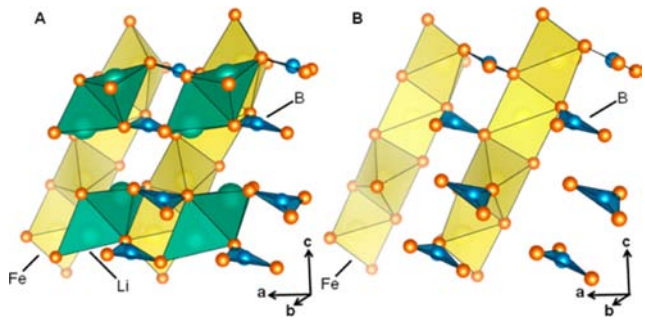

Figure 5. DFT-optimized crystal structures for (A) the $C2/c$ average structure approximant of $LiFeBO_3$, and (B) the unmodulated $C2/c$ symmetry structure of $FeBO_3$ resulting from delithiation.

dx.doi.org/10.1021/ja301881c | J. Am. Chem. Soc. 2012, 134, 12516−12527

geometry. Both starting points gave the same end result (Figure 5, right). The unit cells and atomic coordinates of the unmodulated, modulated, and delithiated structures resulting from these optimizations are given in Supporting Information Tables S7−9.

The geometry optimizations reproduce the experimental structures of $LiFeBO_3$ well, with maximal errors in cell length of 1.4 and 0.8% for unmodulated and modulated forms, respectively, and 0.4 and 2.6% for the respective monoclinic β angles. Optimization of the $C2/c$ structural model leads to an average structure in which the Li atoms move from initial trigonal bipyramidal to tetrahedral coordination, albeit adopting an arrangement of up and down oriented LiO_4 tetrahedra differing from that refined above in the super space group. This result is expected, for the higher symmetry and smaller volume of the $C2/c$ unit cell means that it cannot accommodate the orientation of LiO_4 chains occurring in the modulated structure. While we hold that the experimental $C2/c$ structure provides a good model of the average form of $LiFeBO_3$, optimizations in this symmetry apparently capture most of the local distortions occurring in the refined modulated structure above, differing only in the longer scale arrangement of tetrahedra. Thus, the optimized $C2/c$ structure likely cannot be regarded as representative of the average structure lacking the modulation. It is clear that a broader study of structures bearing a range of tetrahedral arrangements will be required to obtain an "average" energy against which to measure the stabilization of the lattice due to the modulation, a topic for future work.

Delithiation in the present hybrid calculations to form $FeBO_3$ leads to increases of 2.5 and 3.5% in cell volume (relative to $LiFeBO_3$) for $C2/c$ and $P2_1/c$ forms, respectively, in contrast to the experimental observation of an approximately 2% reduction by Yamada et al.,[11] and the previous DFT+U calculations of Seo et al.,[16] which found a 1.4% reduction. It should be noted, however, that a typical error of 1−2% in DFT-derived lattice constants imposes an error of approximately 2−3% in optimized volumes, calling into question the meaningfulness of variations below this level. Certainly, the present calculations confirm the highly desirable trait of $LiFeBO_3$ that it displays only a very minor change in cell volume upon delithiation. The Fe and B atoms in $FeBO_3$ assume positions close to those anticipated for the ideal structure, but the O atoms are shifted slightly from their coordinates in $LiFeBO_3$, to the effect that the BO_3 triangles and FeO_5 trigonal bipyramids are rotated and tilted away from their positions in $LiFeBO_3$, as shown in Figure 5.

Bearing in mind the caveat above, the total energy of the optimized $P2_1/c$ modulated form was found to be marginally lower in energy than that of the $C2/c$ unmodulated structure, but the difference in energy amounts to only 1.2 kJ/mol (12 meV/f.u.), an energy at the lower end of the range from approximately 20 to 140 meV/f.u. associated with varying Li arrangements in partially delithiated Li_xFeBO_3 phases obtained by previous DFT+U calculations.[11] The 1.2 kJ/mol difference is arguably within the normal range of error associated with hybrid DFT energetics.[26] Justification of the comparison of energies in this range, however, can be made on the basis of the similarity of the unmodulated and modulated structures in terms of their Li−O, B−O, and Fe−O connectivities and bond types and also in terms of their electronic structures. In particular, when the optimization of $FeBO_3$ is performed within the different constraints of the $P2_1/c$ and $C2/c$ symmetries, the energy difference between the delithiated forms resulting from $P2_1/c$ modulated and $C2/c$ unmodulated initial structures falls in magnitude to only 0.02 kJ/mol, approaching the tolerance of the calculations and confirming that the small difference in $LiFeBO_3$ energies is driven by the changes in bonding of the Li ions. Since Li−O bonds are, in general, rather weak, it is not surprising that the difference in energy between modulated and unmodulated forms of $LiFeBO_3$ is small, albeit that it corresponds to a difference in the long-range ordering of LiO_4 tetrahedra, as discussed above.

DFT supports the experimental observation that the structural modulation gives the lowest energy ground state, and that the structural and energy differences are small. The latter finding further suggests that the magnitude of the modulation may exhibit substantial temperature dependence, as confirmed by our preliminary experiments, and also that the modulation may be readily disrupted by structural modifications such as substitution at the Fe sites and/or delithiation. Such issues will become particularly relevant to the performance of this material as a cathode if the modulation is found to inhibit Li-ion mobility.

Given the finding that the modulation in $LiFeBO_3$ is driven by the tendency to optimize Li binding, the mobility of Li is expected to be strongly coupled to the structural distortions associated with the modulation, potentially behaving as an ionic polaronic material in the sense that a mobility barrier contribution due to self-trapping must be considered. The discussion above makes plain that the optimized $C2/c$ and $P2_1/c$ structures both serve as the initial or final state for Li ion site hopping. Direct DFT calculations of transition states in the modulated structure are still required. Certainly, the long-range ordering of the Li and O3 distortions suggests that cooperative effects may well be important, and further, that the penalty invoked by a hopping Li ion creating a defect down oriented LiO_4 tetrahedron within a chain of initially only up tetrahedra may be substantially greater than the energy scale of approximately 1 to 2 kJ/mol derived above.

3.6. Chemical Bonding Analysis Using DFT. As noted above, the Mulliken method has been used to partition charge and spin densities into atomic contributions. The absolute values obtained from such analyses must be interpreted with caution, for they are known to display strong basis-set dependence.[32] Their relative variations upon delithiation, however, are expected to be reliable. Table 5 presents the total and unpaired electron occupations averaged over all equivalent species in $LiFeBO_3$ and $FeBO_3$, and the differences that arise due to delithiation. Bearing in mind the caveat above, it is clear that, in comparison with other polyanionic compounds, the absolute Mulliken charges and spins broadly support the $Li^+Fe^{2+}(BO_3)^{3-}$ attribution of formal charges in the

Table 5. Total, $n(\alpha+\beta)$, and Spin Unpaired, $n(\alpha-\beta)$, Mulliken Electron Populations Averaged over Equivalent Species in Optimized $P2_1/c$ $LiFeBO_3$ and $FeBO_3$, and the Differences Arising Due to Delithiation

	$LiFeBO_3$		$FeBO_3$		difference	
atom	$n(\alpha+\beta)$	$n(\alpha-\beta)$	$n(\alpha+\beta)$	$n(\alpha-\beta)$	$\Delta n(\alpha+\beta)$	$\Delta n(\alpha-\beta)$
Li	2.063	0.002	—	—	−2.063	−0.002
Fe	24.162	3.736	23.780	4.277	−0.382	+0.541
B	3.550	0.032	3.740	0.068	+0.190	+0.036
O	9.408	0.077	9.160	0.218	−0.248	+0.141

dx.doi.org/10.1021/ja301881c | J. Am. Chem. Soc. 2012, 134, 12516−12527

lithiated compound. However, the Fe and the BO_3 group charges drop in magnitude to only $\pm 2.2e$ in the delithiated compound. Of the oxidation arising due to the $LiFeBO_3 \rightarrow FeBO_3$ cathode reaction, the Fe atoms contribute 40.8%, the O atoms 79.5%, and the B atoms −20.3% per $FeBO_3$ framework unit, the latter representing an unexpected increase in electron occupation upon oxidation of the phase. For comparison, an equivalent analysis for the olivine-structured $LiFePO_4 \rightarrow FePO_4$ reaction yields contributions 43.9, 11.7, and 44.4% for Fe, P, and O sites, respectively, per $FePO_4$ framework unit.[33] It is apparent that the B sites are significantly reduced upon delithiation of $LiFeBO_3$, as compared with the P sites in $LiFePO_4$, which show partial oxidation. Moreover, the O sites contribute much more substantially to the oxidation of the framework in the former compound as compared with the latter.

Further insight into the evolution in electronic structure due to delithiation emerges from an examination of the Mulliken atomic overlap (or bond) populations. Averaging over all equivalent species in the cell, the Fe−O populations are found to increase from 0.020*e* in $LiFeBO_3$ to 0.031*e* in $FeBO_3$ (both values being close to the notional ionic limit) associated with a reduction of 0.134 Å in mean Fe−O bond length. The B−O populations, meanwhile, show a much more substantial increase from 0.137 to 0.251*e* on delithiation, accompanied by only a small reduction of 0.009 Å in mean B−O bond length. For comparison, the mean Fe−O and P−O overlap populations are 0.019 and 0.262*e*, respectively, in $LiFePO_4$, and 0.040 and 0.257*e* in $FePO_4$. Delithiation therefore yields a significant increase in the covalency of the polyanionic groups in $LiFeBO_3$ as compared with the prototypical $LiFePO_4$ cathode. The stability conferred by the covalency of such groups in the delithiated state is generally regarded as an advantage held by polyanionic compounds over more conventional cathodes such as $LiCoO_2$. Further calculations of the thermodynamics of decomposition[34] and reaction with typical electrolytes are necessary, but the results show promise for the safety of $LiFeBO_3$-based cathodes.

Finally, the atom and spin projected electronic densities-of-states (DOS) of the lithiated and delithiated $P2_1/c$ structures are presented in Figure 6. The electronic structure of $C2/c$ $LiFeBO_3$ disclosed by the DFT+*U* calculations of Seo et al.[16] is broadly reproduced here (Figure 6a), including the narrow Fe-derived e″(β) states (α and β denote majority and minority spin states, respectively, in the ferromagnetic cell) comprising the topmost filled valence bands (VBs), and a band gap of width 3.52 eV in reasonable agreement with the previously computed value of 3.19 eV. Interestingly, the present calculations also yield a narrow gap of width 0.8 eV separating the lowermost filled Fe e″(β) band edge and topmost filled α-bands, the latter comprising a near equal admixture of O- and Fe-derived states. In $FeBO_3$, the absence of the filled Fe e″(β) bands in the DOS plot (Figure 6b) is in agreement with the previous DFT+*U* results, but the population analyses discussed above caution against a rigid band interpretation of framework oxidation purely in terms of the emptying of these states. The key point here is that in strongly correlated materials of this type, the orbital eigenvalues typically vary sensitively with orbital occupation, and profound reorganizations of band structure can be observed, for example, as a result of $d \rightarrow d$ and charge transfer excitations.[35,36] In contrast with the previous assignment,[16] the atomic projections here reveal that the dominant weight of filled Fe(α) states is shifted downward in energy to a range well away from the topmost filled bands (the latter being composed nearly exclusively of O-derived states), consistent with the partial oxidation of Fe sites in $FeBO_3$. The band gap of $FeBO_3$ computed here at 3.26 eV also differs significantly from the much smaller value of 1.59 eV obtained by Seo et al.[16] The discrepancy likely comes from the lack of account for the variation in effective *U* value with the degree of Fe oxidation state in the previous calculations, given that a physically reasonable increase in *U* upon oxidation of Fe sites should lead to a widening of the band gap. Similar DFT+*U* calculations for the $R\bar{3}c$ polymorph of $FeBO_3$ suggest that a value $U = 6$ eV (some 1.7 eV in excess of the value used by Seo et al. for $C2/c$ $FeBO_3$[16]) is necessary to accurately reproduce the experimental band gap.[37]

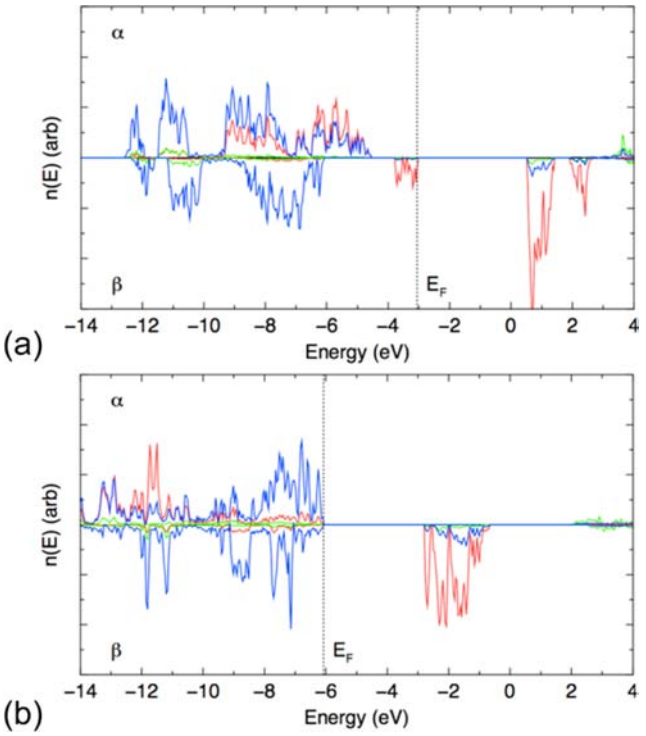

Figure 6. Atom and spin projected electronic densities-of-states [$n(E)$, in arbitrary units] plots versus energy (eV) for $P2_1/c$ (a) $LiFeBO_3$ and (b) $FeBO_3$ in their ferromagnetic states. Majority (α) and minority (β) spin states are plotted separately. Vertical dotted lines mark the energies of the topmost filled states. Black, red, green, and blue lines denote Li, Fe, B, and O contributions, respectively.

3.7. Li-Ion Diffusion Pathways. Although the Li coordination is tetrahedral, it is still convenient to discuss the Li diffusion pathways in terms of trigonal bipyramids. Each trigonal bipyramid may be regarded as two face-sharing tetrahedra, and in stoichiometric $LiFeBO_3$ only one of the two tetrahedra will be occupied by Li. The barriers for Li crossing from one tetrahedral half of the bipyramid to the other are very small relative to other hopping processes, a conclusion supported by prior DFT calculations[16] and our own analysis. Furthermore, when Li leaves the interior of a bipyramid, the distinction between the two tetrahedral halves of the bipyramid is likely lost. For these reasons, the Li diffusion will be examined here in terms of the larger effective LiO_5 trigonal bipyramids rather than the true LiO_4 chemical functional group. This discussion builds on the earlier analysis of Seo et al.,[16] who described and quantified Li diffusion pathways in $LiFeBO_3$

dx.doi.org/10.1021/ja301881c | J. Am. Chem. Soc. 2012, 134, 12516−12527

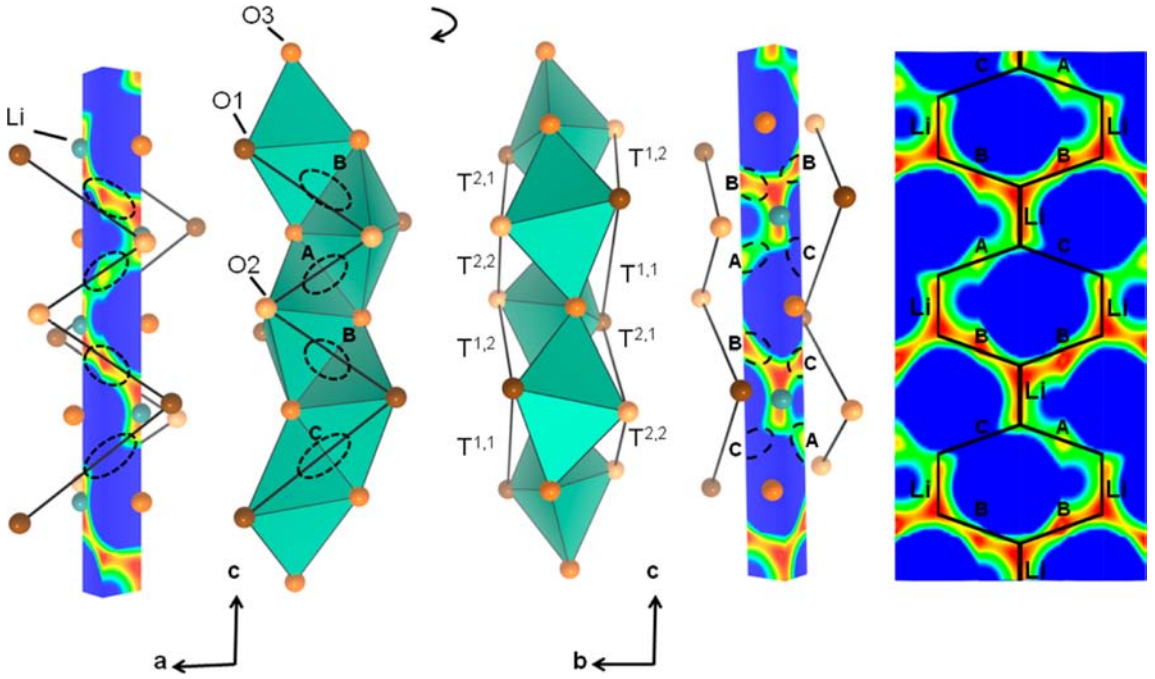

Figure 7. Structural and bond-valence sum analysis of the Li-ion diffusion pathway in the "average" $LiFeBO_3$ structure with $C2/c$ symmetry. Dashed circles indicate the locations of the A, B, and C "tetrahedral" sites external to the edge-sharing LiO_5 polyhedral chains that enable Li-ion diffusion along the [001] chain direction, shown superimposed both onto the polyhedral chains (center of figure, two views rotated by 90°) and onto a tubular square section of the 3D valence map running through the center of the LiO_5 chains shown in the same orientation. The distance between the sections is 1.2 Å, and the colors indicate a ΔV ranging from 0 (red) to 0.16 and larger (blue), with the portions of the map that are not blue representing the lowest energy positions for Li within the $LiFeBO_3$ lattice through which Li can most easily diffuse. Areas A, B, and C are part of the potential diffusion pathway for Li, and correspond to bridging T "tetrahedral" sites that Li might pass through as it diffuses along the [001] LiO_5 chains, as explained in the text and Supporting Information. Right: An unwrapped square tubular section of the Li ΔV map emphasizing the connectivity of low-resistance (A, B) and high resistance (C) diffusion pathways for Li ions that are expected to behave as a chain of parallel pairs of resistors along the 1D tube provided by the LiO_5 chains. Note that an area slightly larger than the full circumference of the tube is displayed to allow the diffusion pathway to be more easily visualized.

based on DFT calculations taking the unmodulated $C2/c$ Legagneur model as a starting point.

In the "average" Legagneur structure of $LiFeBO_3$ which does not consider modulations, the LiO_5 trigonal bipyramids are arranged in isolated edge-sharing chains running along the [001] direction in a zigzag fashion (Figure 7). Since the energy barrier is prohibitively large for Li passing through the shared edges of the bipyramids (which comprise two large O ions in close proximity), the lowest energy pathway for diffusing Li is to leave via a triangular face of one LiO_5 bipyramid and enter the triangular face of a second LiO_5 bipyramid. These two faces define a tetrahedral void external to the LiO_5 chains, and the stability of Li in these tetrahedral sites[38] dictates the activation barrier to Li hopping. Two of the four tetrahedral oxygens (both O3) are common to both LiO_5 faces; the other two "bridging" oxygens (either O1 or O2) can be used to enumerate the four possible types of tetrahedral linkages in this structure which involve bridges of O2−O2, (3.502 Å), O1−O2 (4.312 Å), O2−O1 (4.312 Å), and O1−O1 (5.338 Å). The tetrahedral voids defined by these bridges will be labeled A, B, C in order of increasing bond length, following the notation of Seo et al., where the B-type O1−O2 and O2−O1 tetrahedra are exactly equivalent due to the $C2/c$ symmetry operations.

These tetrahedral voids through which Li traverses occurs in pairs along the LiO_5 chains. The sequence of sites on one side of a [001] LiO_5 chain is ABCBABCB, while on the opposite side, it is CBABCBAB. The A sites are always found opposite of C sites, while B sites are found opposite another B site. Thus, a Li atom moving up or down to the next LiO_5 bipyramid in a chain will have to pass through one site in an [A,C] pair moving in one direction, and one site in a [B,B] pair moving in the opposite direction. The ionic resistance of Li moving within the 1D chains of $LiFeBO_3$ will therefore be analogous to the electrical resistance of pairs of parallel resistors connected in series, where the resistance to Li diffusion of each individual resistor is determined by the Boltzmann weights for the different activation energies of the A, B, and C sites. Both prior calculations[16] and our current BVS analysis find the C site activation energy to be extremely high relative to the other two sites, leading to the conclusion that this site is not part of the Li conduction network at room temperature. Because of the site connectivity, the hopping site with the higher activation between A and B will limit the ionic mobility of Li along the LiO_5 chains in $LiFeBO_3$ in the [001] easy direction.

Just as the presence of a modulation in $LiFeBO_3$ resulted in a 4-fold increase in the number of unique atomic sites, the modulation results in two different types of LiO_5 chains and eight types of Li hopping sites external to the chains, and the details of their arrangement are given as Supporting Information. However, the general features of these sites are unchanged from the average $LiFeBO_3$ structure, enabling the sites to still be classified as A, B, and C with the sequence in which they occur being unchanged (Figure 8). Knowledge of the relative energies of the A, B, and C sites in the presence and absence of the structural modulations will allow the impact of

dx.doi.org/10.1021/ja301881c | J. Am. Chem. Soc. 2012, 134, 12516−12527

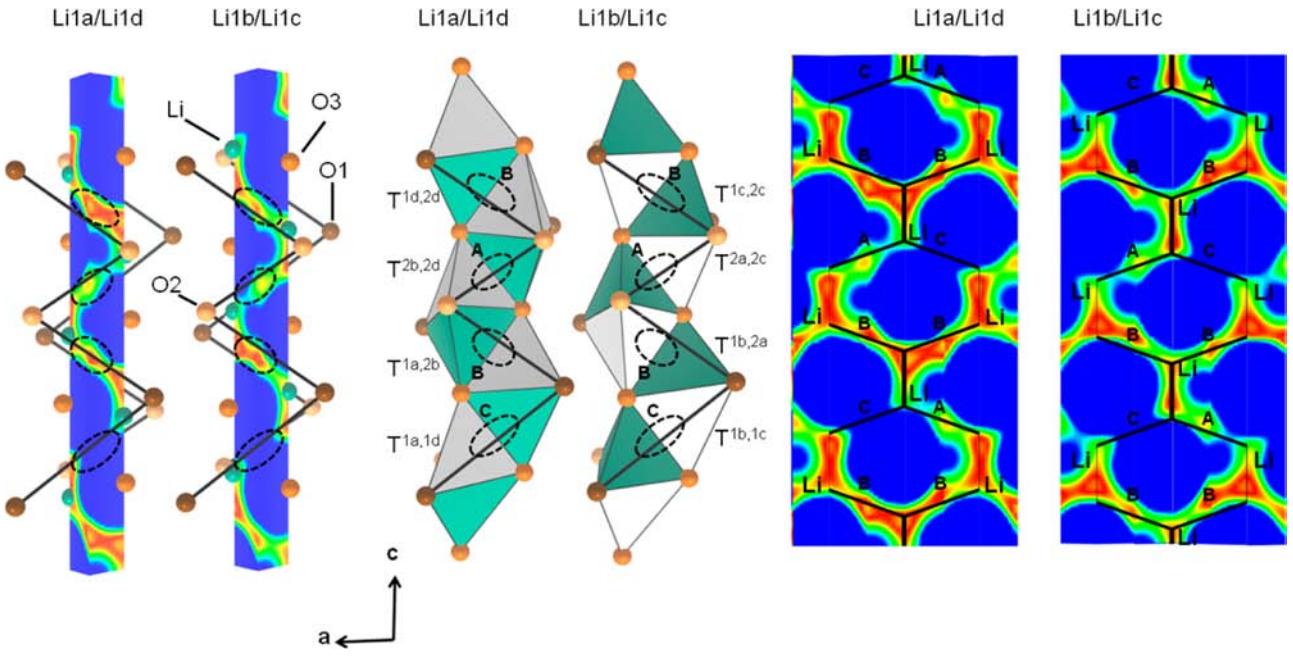

Figure 8. Structural and bond-valence sum analysis of the Li-ion diffusion pathway in each of the two distinct types of LiO_5 polyhedral chains (Li1a/Li1d and Li1b/Li1c) in the modulated structure of $LiFeBO_3$. Center, left: Connectivity for "tetrahedra" involved in Li-ion diffusion, and square sections of the Li bond valence difference map drawn around the center of LiO_5 polyhedral chains. The distance between the sections is 1.2 Å, and the colors indicate a ΔV ranging from 0 (red) to 0.16 and larger (blue). Areas A, B, and C are marked in analogy with the regions defined for the "average" structure, an assignment supported by the very similar shapes and sizes of these "tetrahedra". Right: Unwrapping of the tubular square sections of the bond valence difference map. It can be seen that there are higher barriers for diffusion in the Li1b/Li1c chains even though the same topological network connectivity is found in both chains.

the $LiFeBO_3$ structural modulation on Li-ion mobility to be assessed.

3.8. BVS Map Analysis. A first estimate of the effect of the modulations on Li-ion diffusion can be made using BVS maps.[21,23] The two structures used for comparison were the newly refined $C2/c(^1/_2 00)00$ modulated structure with the atom positions described in the equivalent $P2_1/c$ cell, and an unmodulated average structure obtained by refining our single crystal diffraction data with the constraints of the earlier $C2/c$ space group and with unsplit sites for both Fe and Li. For the results presented here, the absolute difference, ΔV, between the BVS-calculated valence at each grid point (V_{xyz}) and a notional ideal Li valence of +1 was examined. In the resulting 3D maps (Figures 7 and 8), the threshold ΔV value separating accessible and inaccessible Li ion positions was increased until a path connecting different Li sites was found, allowing the percolation threshold to be determined. The value of ΔV at the percolation threshold is expected to be broadly related to the activation energy for ionic mobility,[21] as increasing values of the ΔV threshold clearly represent a larger barrier to Li motion, but there is not an exact theoretical or even empirical relationship relating the activation energy for Li ion hopping to the magnitude of ΔV. The BVS map calculations used as input only the O atom positions and the *SoftBV* parameters provided by Adams[23] that are less sensitive to the chosen cutoff distance (5.5 Å) than the "hard" BVS parameters originally derived by Brown and Altermatt[39] or Brese and O'Keefe.[31] The "hard" parameters require a clearly defined first coordination shell in a manner that is not well-defined for Li ions at positions that are sampled during diffusional hops between resting sites. Since the O positions refined for the average $C2/c$ structure with unsplit sites are very similar to those occurring in the previously reported Legagneur structure, the conclusions of our BVS map analysis for the average structure should apply essentially without modification to the Legagneur model.

The main difference between the modulated and unmodulated structures of $LiFeBO_3$ is the position of the O3 atoms, a difference that is expected to substantially change the calculated ΔV values, and potentially, the Li diffusion mechanism. In contrast, the Fe and B atom positions (and the Li electrostatic repulsion associated with them) are almost unaffected by the modulations. Thus, the calculations analyzed here can be interpreted as providing the effect of the O atom modulations on Li conductivity. Our BVS map analysis identifies the *A* and *B* "tetrahedral" sites to be important for Li motion due to their relatively low energies, consistent with the DFT + *U* results of Seo et al.[16] Also in agreement with Seo et al., we find that the C sites do not substantially stabilize Li and are therefore unlikely to be an active component of the Li diffusion pathway. The BVS maps also suggest that some octahedral sites (interposed between the LiO_5 bipyramidal chains which, if accessible, will enable 3D rather than 1D diffusion of Li) may also be a component of the Li diffusion network, a spurious result which results from the limitations of the BVS methodology. When these octahedral sites were previously investigated by DFT methods, they were found to have a very high activation energy (1.5 eV) for Li motion relative to those of the A (0.22 eV) and B (0.44 eV) sites.[16] This large barrier was attributed to electrostatic repulsion by the adjacent Fe and B cations, interactions which are not considered in the present BVS calculations, the results of which are based solely on O anion positions. It should be noted that a BVS-conduction path for $LiFeBO_3$ has been published before,[40] which appears similar to those calculated here, but that pathway was not analyzed in detail and was based on the published Legagneur structure rather than the present modulated structure.

dx.doi.org/10.1021/ja301881c | J. Am. Chem. Soc. 2012, 134, 12516−12527

Figures 7 and 8 show the Li diffusion pathways identified for the unmodulated and modulated structures, respectively, using the BVS method. The threshold ΔV values that permit diffusing Li ions access to the A and B classes of sites (which represent the relative activation barriers to Li motion) are compared in Table 6. Overall, the paths in the two structures appear very

Table 6. Threshold Values for Bond Valence Difference (ΔV) Needed To Provide Connection between Structural Li Sites Passing through Interstitial Sites of Type A and B, As Defined in the Text[a]

average structure			superstructure		
site	linkage	ΔV (v.u.)	site	linkage	ΔV (v.u.)
A	$T^{2,2}$	0.087	A	$T^{2b,2d}$	0.115
			A	$T^{2a,2c}$	0.117
B	$T^{1,2}$	0.030	B	$T^{1d,2d}$	0.034
			B	$T^{1a,2b}$	0.038
			B	$T^{1b,2a}$	0.049
			B	$T^{1c,2c}$	0.064

[a]The modulated structure clearly exhibits increased barriers for Li diffusion in both types of sites. Notation of linkages is defined in the Supporting Information.

similar, both to each other and to those derived in earlier studies.[16,40] In both the modulated and unmodulated case, the order of thresholds for percolation was $\Delta V_{bipyramidal} < \Delta V_B < \Delta V_A < \Delta V_C$, for the "tetrahedral" A/B/C sites, and for the crossover hop between the "up" and "down" halves of the trigonal bipyramids. This order differs from that derived from the DFT calculations by Seo et al.,[16] who find that pathways involving the A site are lower in energy than those proceeding through the B site. Further DFT calculations are needed to determine if this variation in the observed orders of site energies is due to changes caused by the modulation or due to electrostatic repulsions neglected in the BVS method. For both modulated and unmodulated structures, the threshold $\Delta V_{bipyramidal}$ for crossing between the two halves of the trigonal bipyramid was less than 0.015 v.u., representing a negligible barrier to Li motion in the context of the overall diffusion network.

The percolation thresholds (in units of ΔV) obtained for the modulated structure are all higher than for the average case, suggesting that the modulation substantially inhibits Li motion within the $LiFeBO_3$ framework. The threshold for A sites increases from about 0.09 to 0.12 v.u. on going from the average to the modulated structure. Those of the B site are increased from the average structure value of 0.03 v.u. by 0.005−0.035 v.u. When the connectivity of sites is considered, it is seen that the resistance to diffusion in one modulated structure LiO_5 chain should be substantially higher than in the other, though this effect will have a limited impact on the overall Li mobility since both types of chains run in parallel within the $LiFeBO_3$ structure. It should again be noted that the BVS calculations do not include electrostatic repulsion, so full DFT calculations are necessary to obtain accurate values of activation energies. However, the similarity of the Fe and B cation positions in the modulated and unmodulated test structures suggests that the conclusion that the modulation suppresses Li diffusion rates is robust. The origin of this effect is likely the stronger stabilization of the Li site due to cooperative motions of the Li and O3 atoms.

4. CONCLUSIONS

The structure of $LiFeBO_3$ was redetermined as commensurately modulated with structural refinements in the 4D space group $C2/c(^1/_200)00$, eliminating all of the disorder present when the compound is described in the 3D space group $C2/c$. The modulation was found to primarily consist of motions of the Li atoms away from the centers of their trigonal bipyramids of neighboring O atoms, and the motion of an apical O of the biypramid toward Li, leading to nearly regular LiO_4 tetrahedra that are arranged in an alternating pattern of up and down oriented chains. DFT calculations suggest that the optimized modulated $P2_1/c$ structure is more stable than the similarly optimized unmodulated $C2/c$ form by about 1.2 kJ/mol (12 meV/f.u.). However, the local distortions occurring in both optimized forms are similar, suggesting that this energy difference relates more to variations in the long-range arrangements of the LiO_4 tetrahedra than to a direct measure of the thermodynamics driving the modulation. Bond valence sum maps suggest that Li diffusion is one-dimensional, and allow the network of pathways for Li diffusion to be enumerated. The BVS analysis suggests that the modulation plays a role in hindering Li diffusion within this material, and that full DFT calculations of the activation energies for Li diffusion should be performed again within the revised structural model. It may be possible to enhance Li mobility in this potential Li-ion battery cathode material by elimination of the modulation through substitutional doping or by inducing structural changes that disrupt the long-range order of LiO_4 tetrahedral chains.

■ ASSOCIATED CONTENT

Supporting Information

Derivation, structural parameters, and figure for idealized structure of $LiFeBO_3$; further crystallographic and BVS data for $LiFeBO_3$; enumeration of Li-diffusion pathways in the modulated $LiFeBO_3$ structure; figure of the c-axis view of LiO_4 polyhedra in $LiFeBO_3$; tables of atomic positions for DFT-optimized $LiFeBO_3$ and $FeBO_3$; crystallographic information (CIF) file containing crystallographic data described both in the superspace group and in the space group of the supercell. This material is available free of charge via the Internet at http://pubs.acs.org.

■ AUTHOR INFORMATION

Corresponding Author

cpg27@cam.ac.uk; kpete@bnl.gov

Notes

The authors declare no competing financial interest.

■ ACKNOWLEDGMENTS

This work was supported by the Northeastern Center for Chemical Energy Storage, an Energy Frontier Research Center funded by the U.S. DOE, BES under award No. DE-SC0001294. C.P.G.'s and D.S.M.'s membership of the UK's HPC Materials Chemistry Consortium is gratefully acknowledged, as funded by EPSRC (EP/F067496). This work made use of the facilities of HECToR, the UK's national high-performance computing service, which is provided by UoE HPCx Ltd. at the University of Edinburgh, Cray Inc., and NAG Ltd., and funded by the Office of Science and Technology through EPSRC's High End Computing Programme. The Stony Brook University single crystal diffractometer was

obtained through the support of the National Science Foundation grant CHE-0840483.

REFERENCES

(1) Armand, M.; Tarascon, J. M. *Nature* **2008**, *451*, 652.
(2) Padhi, A. K. *J. Electrochem. Soc.* **1997**, *144*, 1188.
(3) Yamada, A.; Chung, S. C.; Hinokuma, K. *J. Electrochem. Soc.* **2001**, *148*, A224.
(4) Yamada, A.; Chung, S.-C. *J. Electrochem. Soc.* **2001**, *148*, A960.
(5) Manthiram, A.; Goodenough, J. B. *J. Power Sources* **1989**, *26*, 403.
(6) Arroyo-de Dompablo, M. E.; Armand, M.; Tarascon, J. M.; Amador, U. *Electrochem. Commun.* **2006**, *8*, 1292.
(7) Yabuuchi, N.; Ohzuku, T. *J. Power Sources* **2003**, *119−121*, 171.
(8) Legagneur, V.; An, Y.; Mosbah, A.; Portal, R.; La Salle, A. L.; Verbaere, A.; Guyomard, D.; Piffard, Y. *Solid State Ionics* **2001**, *139*, 37.
(9) Dong, Y.; Zhao, Y.; Shi, Z.; An, X.; Fu, P.; Chen, L. *Electrochim. Acta* **2008**, *53*, 2339.
(10) Dong, Y.; Zhao, Y.; Fu, P.; Zhou, H.; Hou, X. *J. Alloys Compd.* **2008**, *461*, 585.
(11) Yamada, A.; Iwane, N.; Harada, Y.; Nishimura, S.; Koyama, Y.; Tanaka, I. *Adv. Mater. (Weinheim, Ger.)* **2010**, *22*, 3583.
(12) Aravindan, V.; Umadevi, M. *Ionics* **2011**, *18*, 27.
(13) Bo, S.; Wang, F.; Janssen, Y.; Zeng, D.; Nam, K. W.; Xu, W.; Du, L.-S.; Graetz, J.; Yang, X.-Q.; Zhu, Y.; Parise, J.; Grey, C. P.; Khalifah, P. G. *J. Mater. Chem.* **2012**, *22*, 8799.
(14) Kim, J. C.; Moore, C. J.; Kang, B.; Hautier, G.; Jain, A.; Ceder, G. *J. Electrochem. Soc.* **2011**, *158*, A309.
(15) Yamada, A.; Iwane, N.; Nishimura, S.-i.; Koyama, Y.; Tanaka, I. *J. Mater. Chem.* **2011**, *21*, 10690.
(16) Seo, D.-H.; Park, Y.-U.; Kim, S.-W.; Park, I.; Shakoor, R.; Kang, K. *Phys. Rev. B: Condens. Matter Mater. Phys.* **2011**, *83*, No. 205127.
(17) Bondareva, O. S.; Simonov, M. A.; Egorovtismenko, Y. K.; Belov, N. V. *Kristallografiya* **1978**, *23*, 487.
(18) Cora, F.; Alfredsson, M.; Mallia, G.; Middlemiss, D. S.; Mackrodt, W. C.; Dovesi, R.; Orlando, R. *Struct. Bonding (Berlin, Ger.)* **2004**, *113*, 171.
(19) Palatinus, L.; Chapuis, G. *J. Appl. Crystallogr.* **2007**, *40*, 786.
(20) Petricek, V.; Dusek, M.; Palatinus, L. *Jana2006. The Crystallographic Computing System*; Institute of Physics: Praha, Czech Republic, 2006.
(21) Brown, I. D. *Chem. Rev.* **2009**, *109*, 6858.
(22) Rodriguez-Carvajal, J.; Gonzalez-Platas, J. *Acta Crystallogr., Sect. A: Found. Crystallogr.* **2002**, *58*, c87.
(23) Adams, S. *Acta Crystallogr., Sect. B: Struct. Sci.* **2001**, *57*, 278.
(24) Adams, S. *J. Solid State Electrochem.* **2010**, *14*, 1787.
(25) Dovesi, R. et al. *CRYSTAL06 User's Manual*; University of Torino: Torino, 2006.
(26) Becke, A. D. *J. Chem. Phys.* **1993**, *98*, 5648.
(27) Muscat, J.; Wander, A.; Harrison, N. M. *Chem. Phys. Lett.* **2001**, *342*, 397.
(28) CRYSTAL Basis Set Repository http://www.crystal.unito.it
(29) Yamamoto, A. *Acta Crystallogr., Sect. A: Found. Crystallogr.* **1996**, *52*, 509.
(30) Villars, P.; Cenzual, K. Pearson's Crystal Data—Crystal Structure Database for Inorganic Compounds, Release 2010/11; ASM International Materials Park: Materials Park, OH, 2010.
(31) Brese, N. E.; O'Keeffe, M. *Acta Crystallogr., Sect. B: Struct. Sci.* **1991**, *47*, 192.
(32) Wiberg, K. B.; Rablen, P. R. *J. Comput. Chem.* **1993**, *14*, 1504.
(33) Clement, R.; Middlemiss, D. S.; Grey, C. P., unpublished work.
(34) Ong, S. P.; Jain, A.; Hautier, G.; Kang, B.; Ceder, G. *Electrochem. Commun.* **2010**, *12*, 427.
(35) Middlemiss, D. S.; Mackrodt, W. C. *Mol. Phys.* **2005**, *103*, 2513.
(36) Middlemiss, D. S.; Mackrodt, W. *J. Phys.: Condens. Matter* **2008**, *20*, 015207.
(37) Shang, S.; Wang, Y.; Liu, Z. K.; Yang, C. E.; Yin, S. *Appl. Phys. Lett.* **2007**, *91*, 253115.
(38) Some "tetrahedra" are not actually tetrahedra due to the close proximity of borate oxygens.
(39) Brown, I. D.; Altermatt, D. *Acta Crystallogr., Sect. B: Struct. Sci.* **1985**, *41*, 244.
(40) Adams, S.; Rao, R. P. *Phys. Status Solidi A* **2011**, *208*, 1746.